High-strength foamed concrete for structural applications: Influence of metakaolin, superplasticizer, maximum fine sand particle size, and dry density

Journal of Building Engineering 113 (2025) 114055

Contents lists available at ScienceDirect

Journal of Building Engineering

journal homepage: www.elsevier.com/locate/jobe

High-strength foamed concrete for structural applications: Influence of metakaolin, superplasticizer, maximum fine sand particle size, and dry density

Peng Shi [a], Devid Falliano [b,*], Qiyun Zhang [b], Giuseppe Carlo Marano [b], Giuseppe Andrea Ferro [b], Luciana Restuccia [b]

[a] State Key Laboratory of Subtropical Building Science, South China University of Technology, Guangzhou 510640, China
[b] Department of Structural, Geotechnical and Building Engineering (DISEG), Politecnico di Torino, Corso Duca degli Abruzzi, 24, 10129, Turin, Italy

ARTICLE INFO

Keywords:
High-strength foamed concrete
Metakaolin
Compressive strength
Elastic modulus
Flexural strength
Lightweight concrete for structural applications

ABSTRACT

Aiming to minimize cement usage and carbon emissions while reducing the weight of structural elements, this work presents preliminary findings from ongoing experimental campaigns focused on foamed concrete for structural applications. This study explores the influence of dry density, superplasticizer dosage, maximum fine sand particle size, and metakaolin on the slump and mechanical properties, including flexural strength, compressive strength, and elastic modulus of foamed concrete. In detail, this experimental study involved the preparation of 90 prismatic foamed concrete specimens with fixed target densities between 1350 and 1600 kg/m^3. All specimens were cured in water for 28 days and subsequently tested according to relevant UNI EN standards. The results show that mixtures containing metakaolin and higher dosages of superplasticizer demonstrate excellent flowability, a crucial characteristic for this type of material in structural applications, effectively eliminating the need for vibration. Additionally, the presence of metakaolin, smaller maximum particle size of aggregate, and higher superplasticizer content can enhance the mechanical properties of foamed concrete by promoting a denser and improved microstructure characterized by smaller micro-air-pore sizes. These conclusions are consistent with the finding related to elastic modulus. Specifically, the maximum compressive strength of the foamed concrete containing metakaolin at a target dry density of 1600 kg/m^3 is approximately 58 MPa, with flexural strength exceeding 8 MPa and an elastic modulus around 20 GPa. The results are promising, in particular the compressive strength is found to be higher than that typical of lightweight aggregate concretes of the same density and is comparable to that of a conventional concrete with strength class C40/50. Additionally, these results underscore the material's strong potential for structural applications. The combination of favorable mechanical properties and reduced density can significantly enhance sustainability in the construction sector by lowering structural dead loads.

1. Introduction

In recent decades, pollution has become increasingly discussed among researchers, especially regarding the effects of greenhouse

* Corresponding author. Politecnico di Torino, Italy.
E-mail address: devid.falliano@polito.it (D. Falliano).

https://doi.org/10.1016/j.jobe.2025.114055
Received 14 February 2025; Received in revised form 15 July 2025; Accepted 8 September 2025
Available online 11 September 2025

Abbreviations

VEA	viscosity enhancing agent
RPM	revolutions per minute
RH	relative humidity
SP	superplasticizer
w/c	water-to-cement ratio
$(w+f)/c$	(water + foam)-to-cement ratio
CH	calcium hydroxide
CSH-I	tobermorite
CoD	coefficient of determination
Std	standard deviation

gas emissions [1,2]. The escalating environmental crisis, particularly the pollution caused by the construction industry, has propelled urgent calls for sustainable and eco-friendly alternatives in construction materials [3,4]. The widespread use of cement, an integral component for concrete production, is among the major contributors to air pollution and the most widely utilized construction material globally [5]. Cement production is a major source of carbon dioxide emissions, energy consumption, and consumption of natural resources [6]. Hence, it has become imperative to explore innovative strategies to reduce cement use while maintaining the structural integrity of the construction materials. The U.S. Geological Survey (USGS) estimates that global cement production reached about 4.1 billion tons in 2020, and global clinker production capacity was around 3.7 billion tons. These figures represent increases of 23.87 % and 19.35 %, respectively, over the previous ten years. The production of 1 kg of ordinary Portland cement (OPC) emits between 0.66 and 0.82 kg of CO_2, accounting for roughly 5–7 % of all anthropogenic CO_2 emissions worldwide [1].

Lately, research has focused on different methods to reduce cement use. One strategy is to employ sustainable materials in concrete production as a replacement for cement. Supplementary cementitious materials, such as blast-furnace slag, fly ash, limestone powder, or calcined clay, have a lower embodied carbon level than standard clinker [3,7]. Another possible strategy is to completely replace Portland cement with aluminosilicate-based materials; in this case, CO_2 emissions can be reduced by up to 80 % compared to OPC. This is because the production of 1 kg of geopolymer emits only 0.18 kg of CO_2, which is merely one-fifth of the emissions generated in OPC production. Another notable strategy is to optimize the structural design in a more efficient manner. Consequently, less material would be required to achieve the desired performance.

Additionally, another alternative to reduce cement use is the employment of foamed concrete. Foamed concrete is a lightweight and low-density concrete variant that reduces the amount of required binder, and therefore, the environmental footprint of concrete [8]. This type of concrete differentiates from regular concrete because it contains micro air-pores. The inclusion of air-pores, achieved through the introduction of a foaming agent, significantly reduces the cement content required while maintaining adequate mechanical strength [9]. This technique offers a viable strategy for minimizing cement usage in construction projects.

Foamed concrete can be used for different applications that vary according to its density. Higher densities, typically ranging from 1200 to 1800 kg/m^3 are aimed for structural applications; medium densities, just as 700–1100 kg/m^3 for non-structural elements; and lower densities between 100 and 600 kg/m^3 for thermal and acoustic insulation [10,11]. In recent years, the use of foamed concrete for structural applications has caught the interest of scientific research. Several studies have been conducted to investigate the performance of foamed concrete in structural elements such as beams, columns, and slabs, demonstrating that foamed concrete can be used to develop structural elements that have the required strength and durability [12].

There are several advantages of applying foamed concrete in structures. To begin with, it can reduce the dead loads due to its lighter weight, which can lead to significant savings in foundation and load-bearing structure costs [13]. In addition, the thermal insulation properties of foamed concrete can contribute to reducing energy costs [8]. Furthermore, this type of concrete requires less cement than traditional concrete to be produced and therefore its application reduces the carbon footprint of the structure. For example, Falliano et al. [14] explored the utilization of structural foamed concrete in seismic-prone regions. In this specific scenario, in a practical case involving a preliminary analysis of a six-story reinforced concrete frame, employing a foamed concrete characterized by a density of 1550 kg/m^3, a substantial enhancement of about 20 % in the principal vibration mode was observed compared to the same model with regular concrete. Furthermore, a noteworthy reduction of approximately 38 % in the maximum shear at the base of the frame was noted.

Despite the advantages of foamed concrete, there are still several challenges that need addressing before it can be widely utilized for structural applications. For example, the microstructure of foamed concrete consists of numerous air pores, whose distribution and size are influenced by various factors such as mixing methods, foaming agent properties, raw materials and mix proportions. Although the topic is highly current, there is limited literature addressing high-performance foamed concrete specifically designed for structural applications. Therefore, this study expands the understanding of foamed concrete for structural applications by examining the effects of maximum fine sand size, metakaolin content, and mix design approach on achieving target density. It specifically analyzes impacts on flexural and compressive strength as well as the elastic modulus at several dry densities, 1350, 1500, and 1600 kg/m^3, and aims to extend what was previously studied in the field of medium-low density foamed concrete [15]. More specifically, unlike the existing literature that often focuses on the use of fly ash and silica fume, this study presents high strength foamed concrete utilizing metakaolin. The results demonstrate that, using the strategies outlined in this study, it is possible to produce foamed concrete with not only

excellent flexural and, especially, compressive strength, but also with an elastic modulus comparable to that of lightweight aggregate concrete, typically used in structural applications. This is an advancement not commonly found in existing literature. These results demonstrate that, from a mechanical properties perspective, the material presented in this study is well-suited for structural applications. Under the optimized mix proportions, the use of metakaolin results in higher load-bearing capacity compared to previous studies utilizing fly ash and silica fume. This study enhances the understanding and research of high-performance foamed concrete for structural applications, providing a promising solution for subsequent uses in structural elements. An upcoming study will further explore the material's durability (e.g., resistance to water penetration, freeze-thaw resistance, resistance to carbonation, resistance to chloride penetration, insulation, and soundproofing) and its bonding performance with reinforcement bars to address any limitations in practical structural applications.

2. Materials and methods

To characterize the foamed concrete presented in this study, prisms of size $4 \times 4 \times 16$ cm^3 were used for the flexural strength and elastic modulus tests, while the compressive strength tests were performed on the two halves obtained as a result of the flexural test. This choice was made in order to save economic costs and raw material usage, and is in accordance with UNI EN 196-1 standard [16]. The entire process of sample preparation and casting is shown in Fig. 1. Ghahremani et al. [17] reported that the compressive strength

Fig. 1. Photographs of foamed concrete preparation.

of cubic foamed concrete samples varied depending on their density and shape. The findings indicated that the strength of the sample with a 5 cm side was about 5 % smaller than that of a usual 15 cm sample, while the strength of the sample with a 10 cm side was about 15 % greater than that of the 15 cm sample.

2.1. Raw materials

The prismatic specimens were cast with Portland cement (PC/CEM I 52.5 R) conforming to UNI EN 197-1 standard [18]; this cement is characterized by a compressive strength greater than 30 MPa after two days of curing, and by a normalized resistance, that is after 28 days of curing, higher than 52.5 MPa. This type I Portland cement with a density of 3100 kg/m^3 was purchased from Buzzi Unicem S.p.A.-Robilante (CN). A natural siliceous sand, with a density of 2760 kg/m^3, was used as fine aggregate. This sand was sieved in order to obtain two different particle size distributions, characterized by two different maximum diameters, i.e. 0.25 mm and 0.5 mm, respectively. This choice was made exactly because one of the purposes of the present work is to highlight the effect of the maximum diameter of the aggregate on the material properties. Moreover, high reactivity metakaolin (HRM) with an amorphous alumino-silicate with a white hue, meeting EN 480–1:2015 [19], was added to the mixtures at a metakaolin-to-cement ratio equal to 43.3:100 to evaluate its possible effect of improving the microstructure of the material through its densifying action. A protein foaming agent, namely Isocem S/B, was obtained from Isoltech s.r.l. Cellular Concrete Technology. It is a dark brown liquid with a specific gravity of 1150 + 0.02 g/L and a pH value of approximately 6–7.5. Additionally, a polycarboxylate superplasticizer provided by Master® Builders Solutions Italy S.p.A., complying with UNI EN 934–2:2012 [20], was used to improve the rheological properties of the foamed concrete. It is a yellow liquid with a relative density 1030–1060 g/L at 20 °C. In addition, a viscosity enhancing agent (VEA) [21] was used to improve the stability of foamed concrete. Mixed water was weighed from local tap water.

2.2. Specimens preparation

In this study, a total of 90 prismatic specimens were produced, 45 samples for flexural strength tests and 45 samples for elastic modulus tests, respectively. A total of 90 samples for compression tests were carried out. Furthermore, the slump value of each sample group was measured before casting. The allowable deviation in the fresh density was limited to ±50 kg/m^3 for each test. Three different target dry densities were prepared, 1350, 1500 and 1600 kg/m^3, with a tolerance of ±50 kg/m^3. Thus, the fresh densities are controlled between 1400 and 1800 kg/m^3. The foam concrete specimens were prepared with the pre-forming method. Specifically, the foam, that was characterized by a density equal to 85 ± 5 g/l, was prepared through the use of the protein foaming agent with a concentration equal to 5 %. Meanwhile, the dry materials were mixed through the use of the mixer shown in Fig. 1 at low speed, equal to 140 rpm, in order to disperse them homogeneously. Subsequently, water and additives were added to the mixture, and it was mixed at high speed, 295 rpm, for about 2 min until a homogeneous paste was achieved. Next, the appropriate amount of pre-formed foam was added to the mixture to form the air voids within the cementitious matrix. At this stage, the mixture of foam and mortar was also stirred for at least 1 min at a speed of 295 rpm, so that the foam was evenly distributed in the mortar. In addition, the fresh density of the mixture was assessed using a pre-weighed measuring cup of known volume. The mix design of the different series presented in this study is reported in Table 1. In particular, cement weight c, water content w, metakaolin dosage m, VEA content v, sand content s, superplasticizer dosage sp, foam amount f, and the relevant proportion w/c, f/c sp/c, and $(w+f)/c$ are indicated for each series. Usually, the higher f/c and $(w+f)/c$ ratios the lower the densities, regardless of wet and dry densities [22]. S1 and S2 in the series label indicate the two different diameters used for fine sand, 0.25 mm and 0.5 mm, respectively; P0 to P3 represent the superplasticizer

Table 1
Mix proportion with respect to cement weight of the tested foamed concrete.

Code ID	Series no.	Sand particle size [mm]	Mix proportion							
			Target density	Metakaolin	VEA	Sand	Water	Foam	Superplasticizer	Ratio 1
			γ_t [kg /m^3]	m/c	v/c	s/c	w/c	f/c	sp/c	$(w+f)/c$
S1P3	#1.1	0.25	1350	0	0.025	2.3	0.45	0.10	0.035	0.55
	#1.2		1500	0	0.025	2.3	0.45	0.03	0.035	0.48
	#1.3		1600	0	0.025	2.3	0.45	0.02	0.035	0.47
S1P3K	#2.1		1350	0.43	0.025	1.8	0.54	0.22	0.035	0.76
	#2.2		1500	0.43	0.025	1.8	0.54	0.14	0.035	0.68
	#2.3		1600	0.43	0.025	1.8	0.54	0.08	0.035	0.61
S1P1K	#3		1350	0.43	0.025	1.8	0.61	0.32	0.015	0.93
S2P0	#4	0.5	1600	0	0.025	2.3	0.45	0.05	0.0075	0.50
S2P1	#5		1600	0	0.025	2.3	0.45	0.01	0.015	0.46
S2P3	#6.1		1350	0	0.025	2.3	0.35	0.06	0.035	0.41
	#6.2		1600	0	0.025	2.3	0.35	0.02	0.035	0.37
S2P2K	#7.1		1500	0.43	0.025	1.8	0.54	0.19	0.02	0.73
	#7.2		1600	0.43	0.025	1.8	0.54	0.17	0.02	0.71
S2P3K	#8.1		1350	0.43	0.025	1.8	0.45	0.22	0.035	0.67
	#8.2		1600	0.43	0.025	1.8	0.45	0.16	0.035	0.61

S1 and S2 denote fine aggregate sands with particle sizes of 0.25 mm and 0.5 mm, respectively; P0, P1, P2, and P3 indicate that the amount of superplasticizer is 0.75 %, 1.5 %, 2.0 %, and 3.5 % of the cement content, respectively; K stands for the presence of metakaolin.

dosages, namely 0.75 %, 1.5 %, 2 %, or 3.5 %, respectively; K refers to the presence of metakaolin the mixture; therefore, if there is no K in the sample label, it means that the sample does not contain metakaolin.

After the preparation, all the specimens were left at a temperature equal to 20 °C, and relative humidity (RH) of 60 ± 10 % for 24 h. The samples were then placed in water and cured at 20 ± 2 °C, as illustrated in Fig. 2.

It is worth noting from Table 1 that the water-to-cement ratio for Series #1 is 0.45, while that for Series #2 is 0.54. This can be attributed to two things: 1) metakaolin is a hydrophilic mineral with high water absorption [23], and 2) metakaolin particles are small and have greater specific surface area and chemical activity, and their introduction results in the formation of more flocculating structures that encapsulate the free water within the slurry [24], leading to an increase in water demand. Comparison of Series #2 and #3 as well as Series #4, #5, and #6 show that the addition of a high superplasticizer dosage is effective in reducing the amount of mixing water. Indeed, in order to achieve good workability, it is necessary to increase the water content or the dosage of superplasticizer [25], despite the grain size of the sand. These additional series thus allow the effect of reducing the water-to-cement ratio and, more in general the water + foam-to-cement ratio, with the concomitant increase in the superplasticizer-to-cement ratio to be evaluated. Furthermore, from the ratios of Series #1 and #6 or Series #2 and #8, it can be found that the water-to-cement ratio of the larger aggregate is lower. This is due to the fact that the maximum particle diameter of the latter (S2) is twice as large as that of the former (S1). Therefore, S1 is characterized by a greater specific surface area and, consequently, a greater demand for water to wet its surface [26]. In any case, comparison between series prepared with different maximum aggregate diameter but same water-to-cement ratio can be made by considering series #2 and #7. Lastly, in order to achieve a certain target density, it can be seen that the water + foam-to-cement and superplasticizer-to-cement ratios are strongly correlated with each other. In particular, a density obtained with a certain water + foam-to-cement ratio and superplasticizer-to-cement ratio can also be achieved by reducing the water + foam--to-cement ratio and, correspondingly, increasing the superplasticizer-to-cement ratio. This is since higher doses of superplasticizers result in better mixture workability, less free water, and improved inter-material compatibility to help to stabilize air bubbles [27,28]. Insufficient water content leads to the matrix to harden causing bubble rupture; too much water content will make the paste too liquid and cannot gather the bubble, resulting in the segregation phenomenon [9,29]. In this regard, the mix designs of S1P3K (#2.1), and S1P1K (#3) at the target density of 1350 kg/m^3, S2P0 (#4), S2P1 (#5), and S2P3 (#6.2) at the target density of 1600 kg/m^3, and S2P2K (#7.2), and S2P3K (#8.2) also at the target density of 1600 kg/m^3, are compared. One of the objectives of this study is to determine whether foamed concrete of the same density, produced through these two different approaches, exhibits distinct mechanical properties. Such differences could potentially favor one mix design approach over the other. Moreover, although a comprehensive assessment of the actual impact of this material in terms of CO_2 emissions requires further investigation, considering various factors such as the potential reduction in structural element cross-sections due to the lower self-weight compared to conventional concrete, the CO_2 emissions associated with the different mix proportions presented in this study are reported here according to a simplified approach. This approach accounts solely for the corresponding CO_2-equivalent emissions per kilogram of each raw material [30–33]. Based on this method, the average CO_2 emissions per cubic meter for the mix designs without metakaolin were approximately 397, 412, and 429 kg CO2e/m^3 for densities of 1350, 1500, and 1600 kg/m^3, respectively. In contrast, the mix designs with metakaolin exhibited average CO_2 emissions of approximately 458, 480, and 490 kg CO_2e/m^3 for the same respective densities. It is worth noting that these values are generally comparable to, or lower than, those typically reported for conventional concrete with compressive strengths in the range of 35–45 MPa, which often range between 350 and 600 kg CO2e/m^3, depending on the specific mix design and cement content.

Table 2 shows the fresh density, at the moment of casting, and the dry density, determined by drying the samples in an oven at 60 °C

Fig. 2. Water curing of part of the samples.

for at least 48 h and, in any case, until a constant weight is reached, as shown in Fig. 3.

2.3. Testing methods

2.3.1. Slump test

Mini slump tests, by means of a mini slump cone characterized by dimensions of 50 mm (top diameter), 100 mm (bottom diameter), and 150 mm (height), were carried out in order to assess the workability and visually evaluate the viscosity of the different series presented in this study [34]. The slump and the horizontal spread in two perpendicular directions were evaluated.

2.3.2. Flexural strength

According to UNI EN 196-1 standard [16], prismatic specimens with size of 4 × 4 × 16 cm^3 were prepared for flexural strength evaluation. The specimens were cured in an appropriate curing water tank at a controlled temperature of 20 °C. After 28 days, flexural tests were carried out using a Zwick/Roell Z050 electromechanical table-top testing machine with a load speed of 50 N/s, as shown in Fig. 4. For each series, three samples were tested, and the mean value, R_f, of flexural strength was computed.

2.3.3. Compressive strength

Tests for the evaluation of compressive strength were performed on the halves obtained from the flexural strength tests. The samples were placed in appropriate frames for the execution of compressive tests through a Zwick/Roell automatic test bench type Zmart.Pro, with a load capacity of 250 kN, as illustrated in Fig. 5, with twin-column steel structure. The loading rate was 2400 N/s, in accordance with the UNI EN 196-1 standard [16]. Six tests were performed for each series, in fact from one prismatic sample it is possible to perform two compression tests, and the peak value of the force of each sample was recorded. The maximum compressive strength, R_c, was then calculated and averaged.

2.3.4. Elastic modulus

The modulus of elasticity, E, is a property, characteristic of the material, which indicates the material's ability to deform elastically. Higher values indicate that the material is stiffer and subject to lower elastic deformation, or, equivalently, that it requires more stress to achieve a certain deformation. The prismatic specimens of 40 mm × 40 mm x 160 mm dimensions were tested through a MTS machine, with a 100 kN load cell, and equipped with a 24-bit acquisition unit. The strain-gauge-based DD1 displacement and strain transducer provides accurate displacement measurements in the range of ±2.5 mm with an HBM accuracy class of 0.1, as shown in Fig. 6. The transducer and amplifier types were SG full bridge direct current voltage, and MX840B, respectively. The excitation voltage taken in the tests was 2.5V. The tests were conducted 28 days after samples preparation; as with the other tests, the samples were cured in water. Three specimens were selected from each series for testing, and the average of their measured values was considered for analysis. The resistive strain gauges were mounted, with a base length of 50 mm, symmetrically on the center lines of two sides of the foamed concrete specimens. Samples were then subjected to three loading and unloading cycles according to the UNI EN 13412:2007 standard [35]. In particular, specimen was loaded, with a loading rate of 0.6 MPa/s, to an initial load value of F_0, corresponding to a stress of 0.5 MPa. This load was kept constant for 60 s, and the corresponding deformation value was recorded, ε_0. Then, an appropriate load, F_a, was reached and applied to induce stress equal to one third of the axial compressive strength of the specimen, f_{cp}, and kept constant for 60 s. Finally the corresponding deformation, ε_a, was recorded. Subsequently, the specimen was unloaded, at the same unloading rate, until the initial load of F_0 was reached, and the previously defined loading cycle was again applied. The samples were subjected to these loading and unloading cycles three times. At the end of the cycles, the samples were tested to obtain the ultimate load, f_{ck}, at a speed of 0.05 mm/min. The modulus of elasticity of the foam concrete can be calculated by the following equations (1) and (2):

Table 2
Density evaluation at different stages.

Code ID	Series no.	Particle size [mm]	Target density γ_t [kg /m^3]	Fresh density γ_f [kg /m^3]	Dry density γ_d [kg /m^3]
S1P3	#1.1	0.25	1350	1518	1378
	#1.2		1500	1663	1531
	#1.3		1600	1744	1630
S1P3K	#2.1		1350	1492	1342
	#2.2		1500	1643	1498
	#2.3		1600	1743	1594
S1P1K	#3		1350	1610	1352
S2P0	#4	0.5	1600	1720	1625
S2P1	#5		1600	1706	1631
S2P3	#6.1		1350	1422	1335
	#6.2		1600	1700	1635
S2P2K	#7.1		1500	1644	1508
	#7.2		1600	1732	1579
S2P3K	#8.1		1350	1502	1365
	#8.2		1600	1719	1579

Fig. 3. Part of the samples employed in this study in the oven, placed in appropriate boxes, for the evaluation of dry density.

Fig. 4. Flexural strength testing frame.

$$E = \frac{F_a - F_0}{A} x \frac{1}{\Delta n} \quad (1)$$

Fig. 5. Compressive strength testing frame.

Fig. 6. Elastic modulus evaluation.

Where E denotes the modulus of elasticity of the foamed concrete; F_a, represents the load when the stress is one third of the axial compressive strength; F_0 refers to the initial load at a stress of 0.5 MPa; A represents the pressure-bearing area of the specimen; Δn indicates the mean value of the difference in deformation between the two sides of the test specimen under the action of F_0 and F_a at the last load cycle.

$$\Delta n = \left(\varepsilon_a^L + \varepsilon_a^R\right)/2 - \left(\varepsilon_0^L + \varepsilon_0^R\right)/2 \tag{2}$$

Where ε_a^L and ε_a^R are the deformation values of the left and right sides of the specimen at F_a loading, respectively; ε_0^L and ε_0^R are the deformation values of the left and right sides of the specimen at F_0 loading, respectively.

2.3.5. Microstructural characterization

The microstructural characteristics of some of the presented foamed concretes, including pore size, and distribution, were evaluated through image analysis performed on slices taken from cubic samples after at least 28 days of air curing. The curing process was conducted at an ambient temperature of 20 ± 3 °C and a relative humidity of 60 ± 5 %. For each series selected, the distribution of air bubbles within the 1 cm × 1 cm cross-sectional area of the samples is evaluated, determining the size of the pores present. This additional evaluation was conducted on selected series to provide further justification for the experimental findings related to mechanical properties.

3. Results and discussions

In this section, the results of slump, flexural strength, compressive strength, and modulus of elasticity measurements for the entire set of foamed concrete specimens are reported. The flexural strength, compressive strength, and modulus of elasticity values for all the different series presented in this study, after 28 days of water curing, are listed in Table 3. In addition to the various observed results, the table also includes statistical data for dry density and mechanical properties, such as standard deviation (Std.). The influences of various dry densities, fine sand grain sizes, presence of metakaolin, superplasticizer dosages, and water dosage on the mechanical behavior was investigated and presented in graphical form. The following subsections provide plots of flexural strength, compressive strength, and modulus of elasticity versus dry density of the specimen for various parameters. The data points marked with markers show the mean values of the corresponding series. The experimental results' dispersion was also quantified and listed using error bars. The corresponding linear regression curves, derived using the least squares minimization method and discussed in detail in the following section, are provided alongside the experimental results for each mechanical property at varying dry densities.

3.1. Slump test

The workability of fresh paste is a critical factor that influences the durability and overall performance of hardened foamed concrete. Table 4 shows the slump values of the foamed concrete series investigated. It is important to emphasize that these tests were conducted on sample series designed to highlight the effects of the presence of metakaolin and the maximum diameter of the fine sand, all while maintaining the same dosage of superplasticizer. Variations in slump values suggest that the consistency of fresh foamed concrete is primarily influenced by the mix design, and differences in its components, such as maximum diameter of the fine sand and foam content [36]. This effect is particularly notable in samples containing metakaolin. The slump of foamed concrete decreases significantly with increasing dry density. Moreover, the increase in fine sand particle size enhances the overall slump by enhancing the inter-aggregate mobility, as shown in Table 4. On the other hand, compared to 0.5 mm fine sand, 0.25 mm fine sand has a greater total surface area, meaning that more water is needed to wet the surface area and maintain the consistency of the fresh mix [36], thereby dropping their slump values. Furthermore, the presence of SPs gives cement particles the same type of charge and forces them to disperse due to electrostatic repulsion [37]. As a result, the free water wrapped in the flocculating structure is released and the flowability of the cement pastes is improved. It's interesting to observe that the compatibility of the foam concrete is greatly improved when metakaolin is used to replace part of the fine sand (see Fig. 7). Specifically, the fluidity of the metakaolin-containing foamed concrete samples quickly spreads along the platform after the device is pulled out, especially for lower densities, indicating that it possesses exceptional workability. This experimental evidence is very important because it highlights how such a material can be

Table 3
Experimental results on the flexural strength, compressive strength, and elastic modulus for each series of foamed concrete.

Code ID	Series no.	Sand particle size [mm]	Mean dry density γ_d [kg/m^3]	Std. dry density σ_{γ_d} [kg/m^3]	Mean flexural strength R_f [MPa]	Std. flexural strength σ_{R_f} [MPa]	Mean compressive strength R_c [MPa]	Std. compressive strength σ_{R_c} [MPa]	Mean elastic modulus E [GPa]	Std. elastic modulus E [GPa]
S1P3	#1.1	0.25	1378	21	5.13	0.15	27.55	1.38	12.54	1.09
	#1.2		1531	19	6.7	0.09	37.88	1.52	16.76	0.88
	#1.3		1630	18	7.72	0.11	45.16	2.15	18.40	1.03
S1P3K	#2.1		1342	8	6.64	0.34	28.51	2.06	13.88	0.45
	#2.2		1498	3	7.35	0.33	44.38	1.55	16.81	0.78
	#2.3		1594	13	8.19	0.42	57.21	1.77	19.65	0.23
S1P1K	#3		1352	16	4.75	0.33	28.07	1.49	11.17	0.16
S2P0	#4	0.5	1625	22	5.74	0.05	34.49	1.56	18.10	0.28
S2P1	#5		1631	6	6.18	0.23	37.39	1.58	18.76	0.43
S2P3	#6.1		1335	10	5.00	0.53	22.59	1.33	12.17	0.26
	#6.2		1635	5	7.28	0.23	38.34	2.40	18.06	0.91
S2P2K	#7.1		1508	22	5.74	0.51	44.86	1.30	17.11	1.27
	#7.2		1579	12	6.15	0.12	48.49	1.59	18.57	0.56
S2P3K	#8.1		1365	1	5.21	0.47	27.48	2.07	12.70	0.24
	#8.2		1579	2	6.76	0.32	48.75	1.56	18.95	0.54

Note: P0, P1, P2 and P3 denote mixes with superplasticiser additive doses of 0.75 %, 1.5 %, 2.0 % and 3.5 % by weight of cement, respectively, while S1P3 and S1P3K denote whether the composition of the mix contains metakaolin replacing some of the fine sand content. S1 and S2 represent sand sizes of 0.25 and 0.5 mm, respectively.

Table 4
Slump values of foamed concrete at various fresh densities.

Code ID	Fresh density γ_f [kg /m^3]	Dry density γ_d [kg /m^3]	Slump [mm]	Std. slump [mm]	Flow [mm]			
					Top	Std.	Bottom	Std.
S1P3	1518	1378	102.0	1.0	105.5	1.5	150.0	2.0
	1663	1531	41.5	0.5	48.5	1.5	109.0	1.0
	1744	1630	31.3	0.8	44.5	0.5	105.5	1.5
S1P3K	1492	1342	144.0	1.0	291.5	1.5	305.3	1.3
	1643	1498	139.5	0.5	232.5	2.5	266.8	1.8
	1743	1594	121.5	1.0	172.0	4.0	208.5	2.5
S2P3	1422	1335	119.5	1.5	107.5	1.5	196.0	1.5
	1700	1635	106.5	0.5	68.3	4.3	154.5	0.5
S2P3K	1502	1365	147.3	0.8	303.5	1.5	318.3	2.8
	1719	1579	140.0	2.0	251.0	3.0	276.5	2.5

Annotate: The slump and flow values of the foam samples at each fresh density were read in at least two different directions and then averaged.

referred to as self-compacting foamed concrete. This property is particularly crucial for structural applications, as it enhances adhesion with reinforcement bars, even when a high density of bars is present. Importantly for this type of material, it also eliminates the need for vibration. Metakaolin's particles are usually finer and more regular in shape than fine sand or even cement [38], and these help to improve flowability by reducing internal friction. Additionally, the replacement of fine sand with metakaolin results in an increase in its fineness modulus, providing more lubrication per unit of specific surface area of the aggregate [39].

Some active sites on the surface of the metakaolin form a stable dispersion system by reacting with the cement slurry, enhancing the stability of the foam and making the structure work better. The introduction of metakaolin in favor of improving the workability of foam concrete is also in agreement with the findings of Dinakar and Manu [40].

3.2. *Flexural strength*

The effects of metakaolin inclusion, sand particle size, superplasticizer and water content on the flexural strength of foamed concrete are discussed in this section.

As expected, see Fig. 8, regardless of other parameters, an increase in the dry density of foamed concrete inevitably leads to an increase in flexural strength. The flexural strength of S1P3K and S1P3 at a dry density of about 1600 kg/m^3 was improved by 23.2 and 50.5 %, respectively, compared to that at around 1350 kg/m^3. For S2P3K and S2P3 specimens, the flexural strength at 1600 ± 50 kg/m^3 was also enhanced by 29.7 % and 45.6 % compared with the dry density of 1350 ± 50 kg/m^3. This is due to the fact that a decrease in the density is linked to an increase in the foam content, resulting in the structure being filled with an increased volume of micro air pores and, consequently, in a reduction per unit volume of the cementitious matrix, which reduces the overall compactness and affects the overall strength development. Among the various mix design strategies aimed at achieving a specific target density, it emerges that the most effective approach for enhancing the flexural strength of foamed concrete involves increasing the superplasticizer-to-cement ratio. This approach is accompanied by a simultaneous reduction in the water + foam to cement ratio, which contributes to improved mechanical performance. This contrasts with the findings of other authors, who suggest that using relatively high dosages of superplasticizer can result in greater instability, leading to poorer microstructure and reduced performance in foamed concrete [29,41]. To further support this claim, it is important to emphasize that this experimental finding was consistently observed across all conditions under which this alternative approach was examined: i) with metakaolin at a target density of 1350 kg/m^3 and a maximum aggregate diameter of 0.25 mm (comparison between S1P3K #2.1 and S1P1K #3); ii) without metakaolin at a target density of 1600 kg/m^3 and a maximum aggregate diameter of 0.5 mm (comparison among S2P0 #4, S2P1 #5, and S2P3 #6.2); and iii) with metakaolin at a target density of 1600 kg/m^3 and a maximum aggregate diameter of 0.5 mm (comparison between S2P2K #7.2 and S2P3K #8.2). Furthermore, the beneficial influence of the superplasticizer is further confirmed by the results obtained for specimens incorporating metakaolin. As shown in Fig. 8, these specimens, indicated by data points ranging in color from light to deep red, exhibit a consistent increase in flexural strength as the superplasticizer content rises from 1.5 % to 3.5 %. This trend is observed regardless of variations in sand particle diameter, underscoring the dominant role of the superplasticizer in enhancing mechanical performance. This result suggests that, in terms of flexural strength, it is more effective to achieve a target dry density by increasing the superplasticizer-to-cement ratio while simultaneously reducing the water-to-cement ratio. This is confirmed, as highlighted before, also in the absence of metakaolin. This happens because, the superplasticizers improves the overall fluidity of the matrix enabling a reduction in the required mixing water, thereby lowering the effective water-to-cement ratio [20,42]. Nevertheless, dry hard concrete mixtures with low water-to-cement ratios have less free water, which results in fewer pores remaining in the cementitious matrix after it has hardened, making it denser and stronger.

Additionally, it is observed that the overall flexural performance of the foamed concrete improves when a portion of the fine aggregates is replaced with metakaolin. For instance, the specimen identified as S1P3K exhibits higher flexural strength compared to the specimen S1P3, as illustrated in Fig. 9. This is because adding metakaolin particles increases the internal connectivity of the foam concrete, making it more difficult for the concrete to fracture under stress and thus improving flexural properties. Another plausible explanation lies in the filler effect of the metakaolin: the fine particles partially occupy voids within the cementitious matrix, promoting internal densification and reducing the presence of microstructural defects [29].

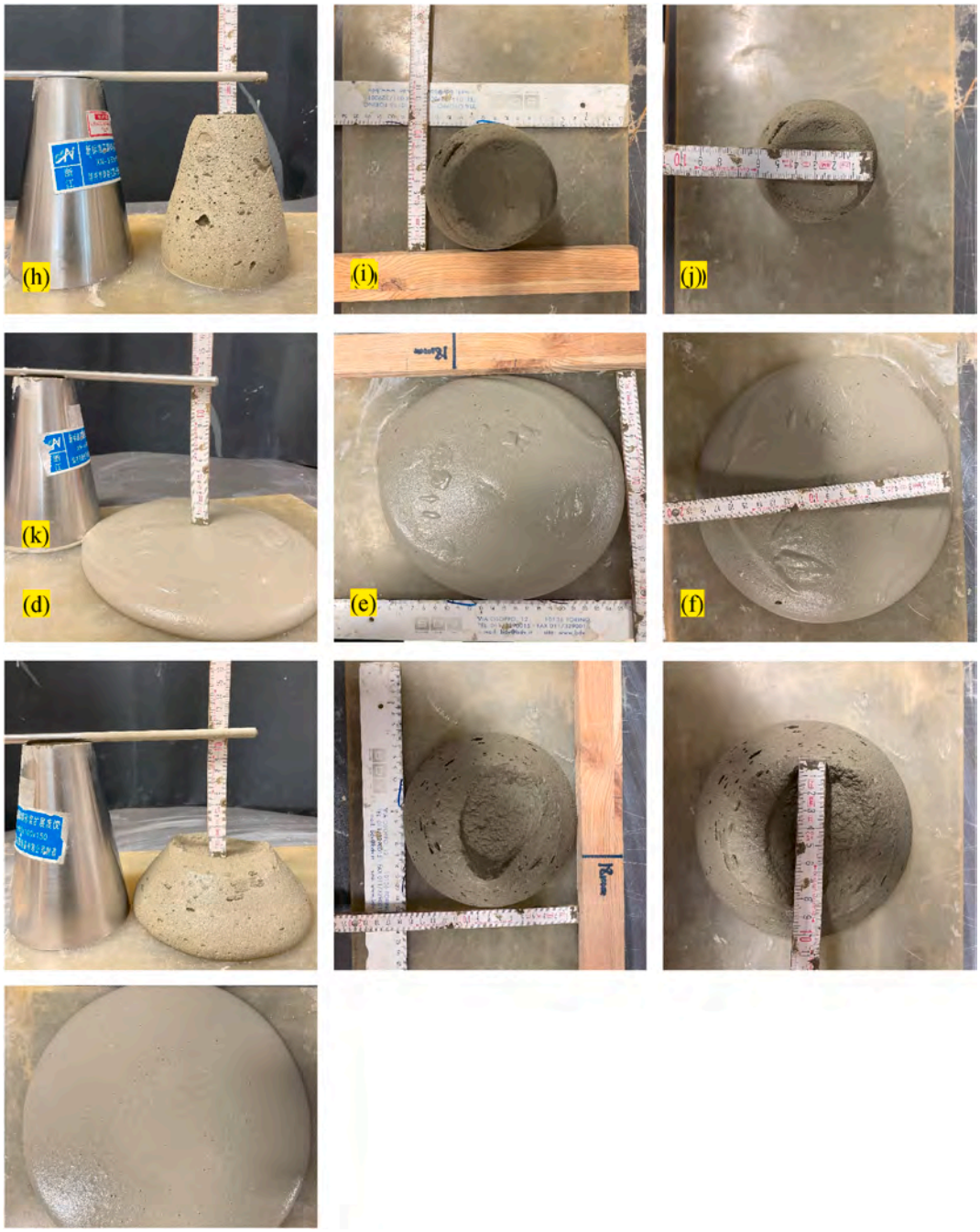

Fig. 7. Slump values of foamed concrete for different maximum fine sand particle size and with or without metakaolin. (ãc) S1P3; (d ~ f) S1P3K; (h ~ j) S2P3; (k) S2P3K.

With regard to the effect of maximum particle size, increasing the fine sand grading from 0.25 mm to 0.5 mm resulted in a reduction in the flexural strength of the foamed concrete (e.g., S2P3K). This weakening can be attributed to the reduced internal support offered by the coarser particles compared to finer grains, which compromises the integrity of the matrix and facilitates the propagation of cracks [43]. As evidenced by the data, the increased total surface area associated with finer sand particles enhances the bonding between the hydrated cement paste and the fillers. This improved interaction strengthens the connection between the fine sand and the cementitious matrix, thereby contributing to greater shear resistance and enhanced flexural performance of the prism specimens. Ultimately, this leads to an overall increase in flexural strength [44]. Similar to compressive strength, smaller micropores contribute to higher flexural strength in foamed concrete. When a specimen is subjected to bending, the outer layers experience tensile and compressive stresses. Smaller pores in the material create a more homogeneous microstructure, which is better able to resist these

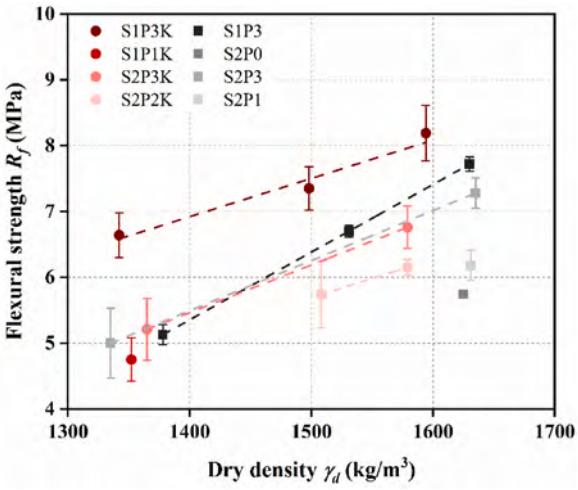

Fig. 8. Effect of dry density on flexural strength for the different foamed concrete investigated.

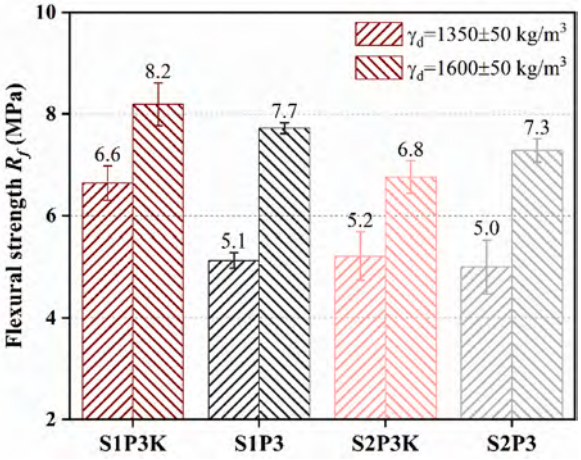

Fig. 9. Effect of the maximum fine sand particle size and of the presence of metakaolin on the flexural strength of foamed concrete at a target density of 1350 ± 50 kg/m^3 and 1600 ± 50 kg/m^3.

stresses. The smaller pore size increases the material's internal cohesion, making it more difficult for cracks to initiate and grow. In samples with larger pores, the stress concentration at the pore boundaries is more significant. This can lead to the formation of cracks at lower bending loads, reducing the overall flexural strength. For example, when comparing samples with different aggregate sizes, the ones with finer aggregates (e.g., 0.25 mm) generally have smaller pores and higher flexural strength. The finer aggregates provide a larger surface area for the cement paste to bond with, resulting in a more compact structure with smaller pores. As shown in the study, for S2P3K specimens, when the fine sand grading is 0.25 mm, the flexural strength is higher compared to when the grading is 0.5 mm. Furthermore, in a bending scenario, an uneven pore distribution and connecting holes can cause the material to deform non-uniformly (e.g., low density or without metakaolin). This non-uniform deformation leads to stress concentrations at the interfaces between regions with different pore densities and creates some microcracks, which then propagate under further loading, reducing the flexural strength. Moreover, another possible cause may be that the presence of aggregates characterized by a larger maximum diameter result in the formation of micropores of a larger size, as will be further illustrated later in this study. The presence of larger pores is in fact generally associated with worse mechanical performance, as the pores can be thought of as defect inclusions within the cementitious matrix. In section 3.3, reliability can be verified also by the specific outcomes of compressive strength.

3.3. *Compressive strength*

Fig. 10 shows the compressive strength of foamed concrete against the various dry densities, and the relationship between flexural and compressive strengths. This study highlights, across the different densities examined, the effects on compressive strength of: i) replacing fine sand with metakaolin; ii) different mix design approach for achieving a specific target density (in terms of water + foam-

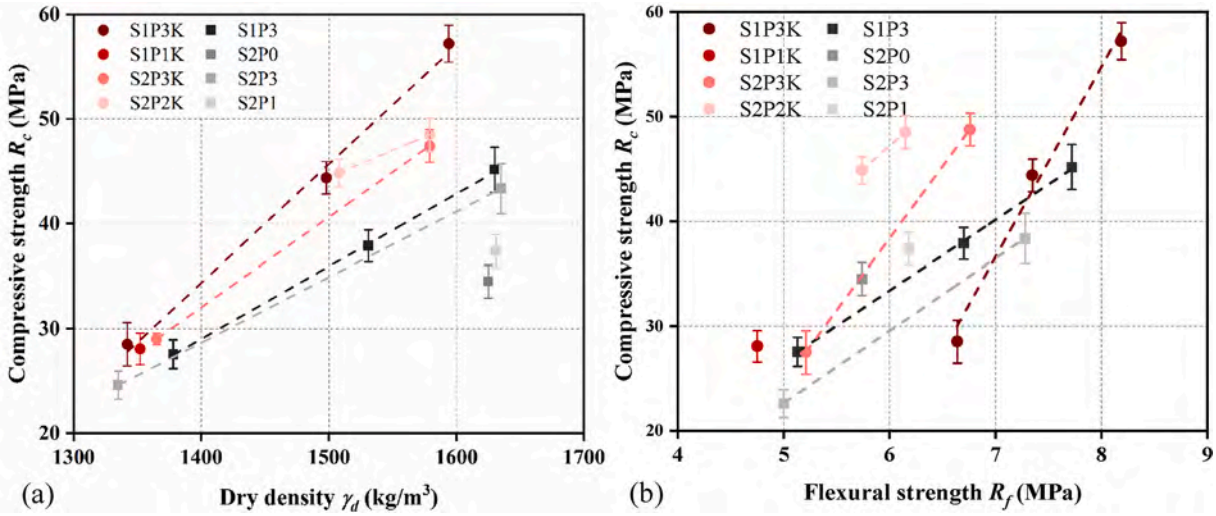

Fig. 10. Effect of dry density on compressive strength for the different foamed concrete investigated (a); flexural strength versus compressive strength (b).

to-cement and superplasticizer-to-cement ratios); and iii) influence of maximum fine sand particle size. In addition to the obvious observation that compressive strength increases as density increases [29], it is very evident that the compressive strength of the samples containing metakaolin (i.e., red round points) is higher than that of the unsubstituted samples (i.e., grey square points). Therefore, in terms of the effect of partially replacing fine sand with metakaolin, significant increases in compressive strength were recorded in all cases analyzed. In particular, in presence of metakaolin, increases of 3.5 %, of 17 % and of 27 % were recorded for target densities of 1350 kg/m^3 (see S1P3 #1.1, S1P3K #2.1), 1500 kg/m^3 (see S1P3 #1.2, S1P3K #2.2) and 1600 kg/m^3 (see S1P3 #1.3, S1P3K #2.3) respectively. According to view of Nambiar and Ramamurthy [44], finer filler materials aid to create a more homogeneous and narrower distribution of artificial bubbles, resulting in improved compressive strength. Moreover, it is well established that metakaolin, a widely available clay mineral, has broad and significant applications in cementitious materials. This is primarily due to its effective filler properties and high pozzolanic reactivity, which enable it to participate in cement hydration reactions. As a result, metakaolin contributes to the formation of additional hydration products analogous to those generated by cement itself, thereby enhancing the strength development of foamed concrete [45,46]. In detail, the amorphous aluminosilicate ($Al_2O_3 \cdot 2SiO_2$) component of the metakaolin with gelling-active and low-crystallinity combines with calcium hydroxide (CH) created via cement hydration to form additional phases such as tobermorite (CSH-I) and hydrated calcium aluminum melilite ($Ca_2Al_2SiO_2(OH)_{10} \cdot 2.25H_2O$). Therefore, the replacement of fine sand by metakaolin enhances the strength of concrete. Furthermore, these findings align with those reported in Ref. [45], where the use of mineral additions – in that case, fly ash – led to significant increases in the compressive strength of foamed concrete for structural applications. However, at the same density, the compressive strength observed in that study was still notably lower than the values achieved in the present work.

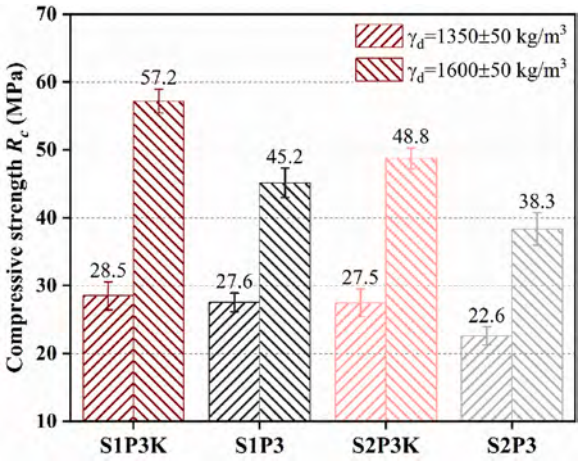

Fig. 11. Effect of the maximum fine sand particle size and of the presence of metakaolin on the compressive strength of foamed concrete at a target density of 1350 ± 50 kg/m^3 and 1600 ± 50 kg/m^3.

Concerning the effect of the mix design approach, slight improvements were again observed when the superplasticizer-to-cement ratio was increased alongside a corresponding decrease in the water + foam-to-cement ratio. However, unlike the findings for flexural strength, where the improvements were significant from an engineering perspective, the gains in compressive strength here are minimal, ranging from only 1 % – 3 %. Notable increases in compressive strength – between 8 % and 11 % – are observed only in cases without metakaolin, attributed to this approach (see S2P0 #4, S2P1 #5, and S2P3 #6.2). It is therefore believed that, when the microstructure is already optimized by the presence of metakaolin, this design strategy offers minimal benefits. In contrast, the advantages become more substantial when the microstructure has greater potential for improvement.

The increase of superplasticizer content in low-size fine sand promotes the compressive strength by improving the fluidity of the paste and the compatibility of the foam concrete while maintaining the same dry density [26,27]. As previously mentioned, the introduction of superplasticizers may lead to issues with bubble stability [38]; therefore, using an appropriate foaming agent or adding a fluorinated surfactant may further improve the stability of the foam [47] as demonstrated also by the present study.

As shown in Fig. 11, the effect of maximum aggregate diameter is most pronounced at the highest density examined, 1600 kg/m^3. This effect is confirmed in both samples with and without metakaolin. In samples with metakaolin, reducing the maximum aggregate diameter from 0.5 mm to 0.25 mm results in an increase in compressive strength of approximately 17 %, while in those without metakaolin, the increase is about 18 %. Similar trends are observed at the lowest density tested, 1350 kg/m^3, where reductions in maximum aggregate diameter led to compressive strength gains of 4 % with metakaolin and 22 % without. Overall, using a smaller maximum aggregate diameter positively impacts the compressive strength of foamed concrete intended for structural applications.

This effect can be attributed to the finer aggregate gradation, which promotes a more optimized and uniform pore structure within the cementitious matrix. Additionally, the increased specific surface area of the finer sand enhances particle-paste interaction, resulting in improved cohesion and reduced susceptibility to segregation. A porous medium's density is typically determined by the quantity and distribution of its pores. Narayanan et al. [48] and Kearsley et al. [49] have concluded that smaller pore volume as well as lesser number of pores results in higher compressive strength. On the other hand, while larger particles can offer improved internal support, their overall impact on the mechanical properties of the concrete is not entirely beneficial. Variations in particle size distribution and morphology may introduce heterogeneity within the internal structure of the material, leading to a less uniform pore network characterized by larger pore diameters. This, in turn, can compromise the overall mechanical performance of the foamed concrete.

In this context, it is noteworthy that a strong correlation exists between compressive strength values and the average diameter of micro air-pore distribution within the cementitious matrix. The values of average diameters were obtained through observations made with the Hyrox RTX-100 optical microscope, see Fig. 12, on sections cut from the different series analyzed, Fig. 13. The image analysis was conducted using Hyrox software. This analysis demonstrates that enhanced compressive strength is linked to the presence of smaller air micropores, Fig. 14, which contribute to an improved microstructure of the material. As shown in this study, these improvements can be achieved by incorporating metakaolin and reducing the maximum aggregate diameter.

In fact, it is widely known that smaller micropores are strongly associated with higher compressive strength in foamed concrete. When the pore size is reduced, the solid matrix between the pores becomes more continuous and structurally robust. This means that when a compressive load is applied, the material can distribute stress more effectively. Larger pores act as stress concentrators and under compression, the stress is concentrated around these large voids, making it easier for cracks to initiate and propagate. For example, in the samples studied (see Fig. 13), those with metakaolin addition often had smaller micropores. Metakaolin reacts with the cement hydration products, forming additional phases like CSH-I and hydrated calcium aluminum melilite. These new phases fill the voids, reducing the pore size. As a result, the compressive strength of samples containing metakaolin, such as S1P3K series, is significantly higher compared to samples without it at the same dry density. The data shows that at a target dry density of 1600 kg/m^3, the compressive strength of S1P3K #2.3 is 57.21 MPa, while that of S1P3 #1.3 is 45.16 MPa. This difference can be attributed, at least in part, to the smaller pore size in the S1P3K sample. Besides, in a material with uniformly distributed pores, the stress is evenly spread

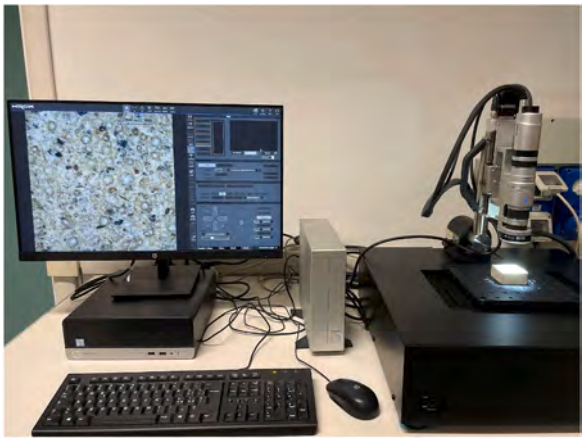

Fig. 12. Pore microstructure analysis by Hyrox RX-100 microscope.

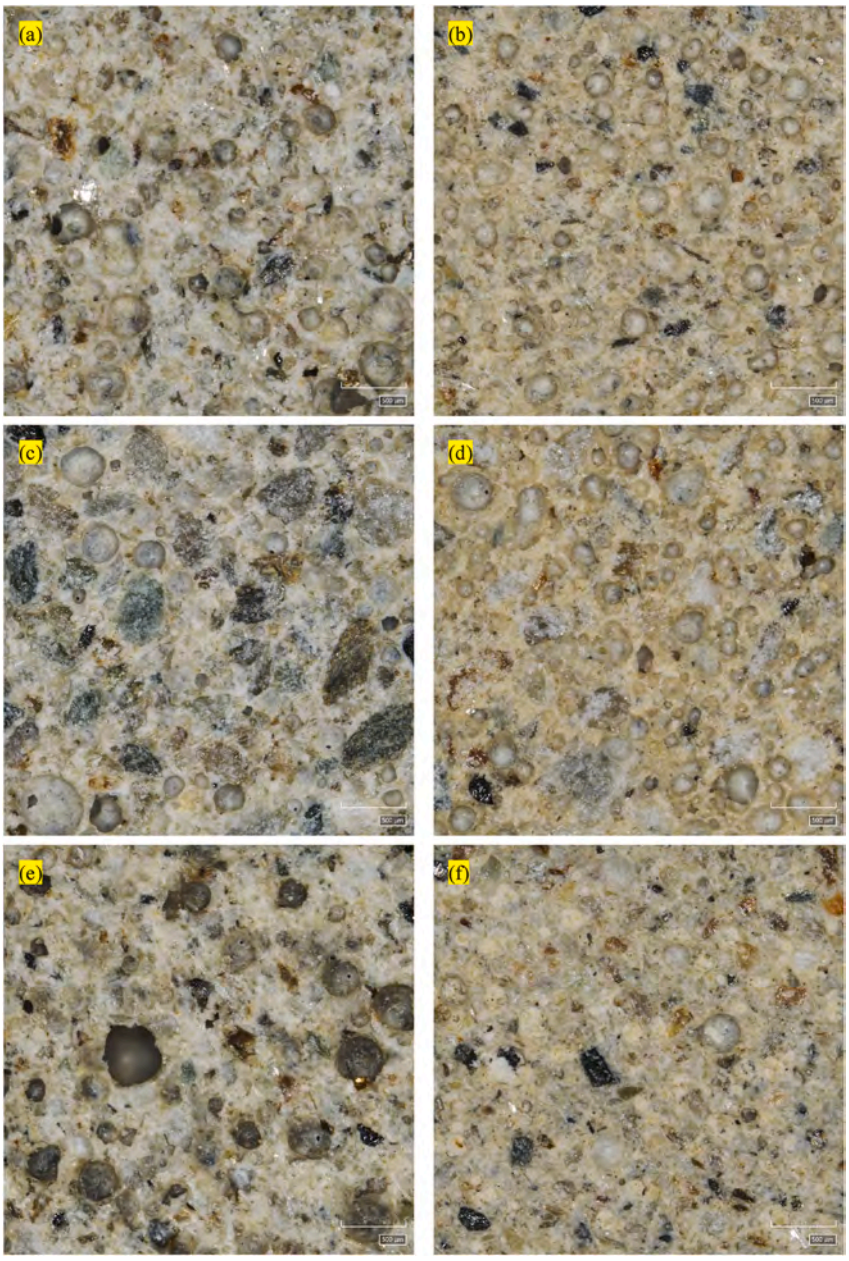

Fig. 13. Microscopic morphological structure of foamed concrete. (a) S1P3_1350; (b) S1P3K_1350; (c) S2P3_1350; (d) S2P3K_1350; (e) S1P3_1500; (f) S1P3K_1500; (g) S1P3_1600; (h) S1P3K_1600; (i) S2P3_1600; (j) S2P3K_1600.

across the structure when a compressive load is applied. This prevents the formation of weak spots that could lead to premature failure, as reported on Fig. 14. When pores are unevenly distributed, areas with larger or more concentrated pores will experience higher stress levels. These areas are more likely to undergo plastic deformation or cracking under load. For instance, if large pores are clustered in one region of the foamed concrete, the material in that region will be less able to support the load, causing the overall compressive strength of the material to decrease. The incorporation of metakaolin enhances both the hydration reactions and the filler effect within the cementitious matrix. This dual contribution leads to a more uniform distribution of micro pores and a significant reduction in pore connectivity. Lower pore connectivity is advantageous, as it not only improves compressive strength but also increases the material's resistance to crack propagation. Also, an appropriate amount of superplasticizer and finer aggregate particle size tends to refine the pores. This is because the superplasticizer improves the compatibility of the mixture, leading to better dispersion of the foam and the formation of more uniform pores.

A linear relationship was found by comparing flexural and compressive data fits, indicating the consistency of the effect of the

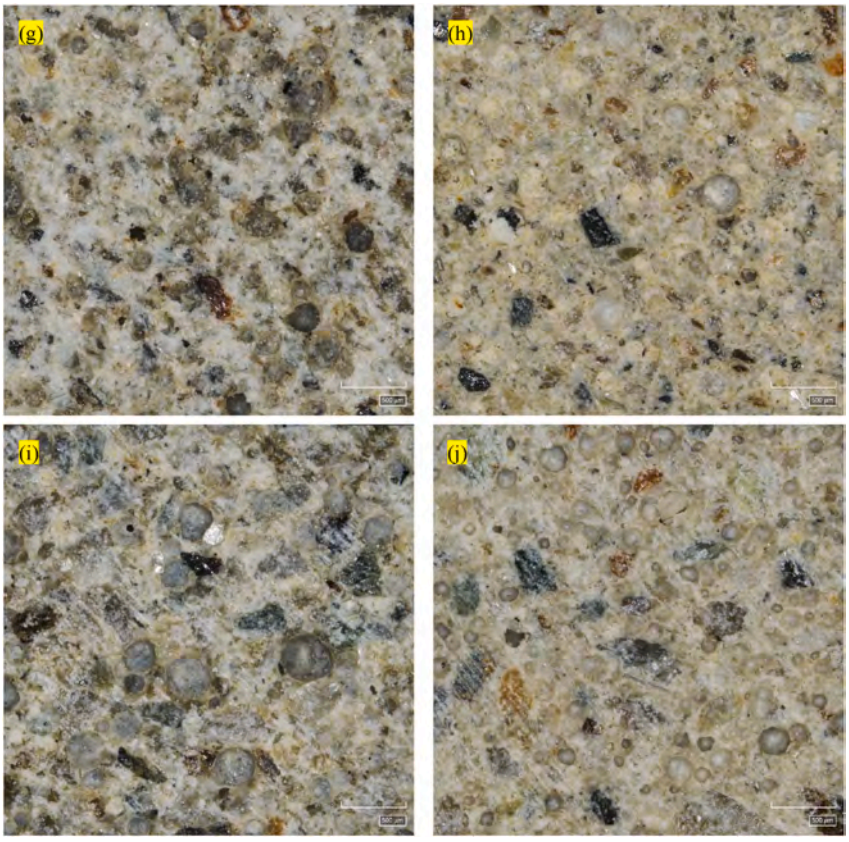

Fig. 13. (*continued*).

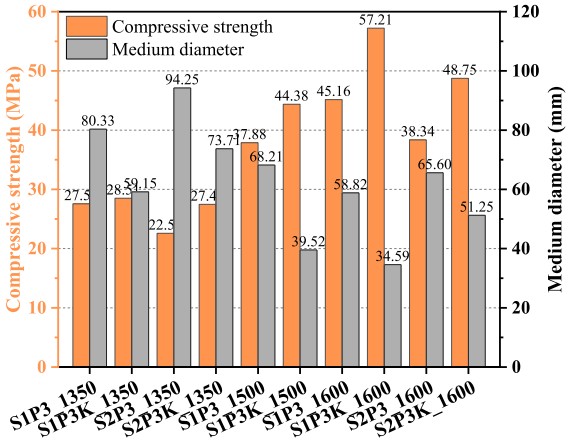

Fig. 14. Compressive strength and medium diameter of air-pores of foamed concrete.

variation of the extrinsic covariates on the mechanical behavior of the foam concrete for each series, as illustrated in Fig. 10(b).

It is noteworthy that the results presented in this study for compressive strength are higher than those reported in the relevant literature. For instance, the best results cited in Ref. [46] indicate compressive strengths of less than 30 MPa at a density of 1600 kg/m^3 and slightly over 20 MPa at a density of 1400 kg/m^3 at 28 days. In contrast [13], reports compressive strengths of approximately 45 MPa at a density just above 1500 kg/m^3 when mineral additives (specifically silica fume) are included, and just over 35 MPa at the same density without mineral additions. In Ref. [50], the compressive strengths of foamed concrete presented for structural use do not exceed 35 MPa at 90 days.

3.4. Elastic modulus

Fig. 15 shows the variation in elastic modulus as a function of density for the different foamed concretes investigated in this study. It may be inferred that an inverse relationship exists between the foam dosage and the modulus of elasticity. Specifically, higher dry density corresponds to a lower foam content, which in turn is associated with an increased modulus of elasticity. Overall, the foamed concrete specimens containing metakaolin (represented by circular markers) exhibited a higher modulus of elasticity compared to the group without metakaolin replacement (represented by rectangular markers), when the dry density was maintained at a constant value. The results of the elastic modulus of foamed concrete align with the trend observed in compressive strength. As previously mentioned, the inclusion of metakaolin consistently enhances the elastic modulus across all cases investigated. Specifically, this improvement corresponds to an average increase of approximately 6 % across the various evaluations conducted. The observations concerning the effect of maximum aggregate diameter similarly extend to the elastic modulus. Although the use of smaller maximum particle sizes yields slight improvements, these increases remain marginal. As illustrated in Fig. 16, when the target dry density of the foamed concrete is maintained at 1600 ± 50 kg/m^3, the enhancement in the modulus of elasticity resulting from the incorporation of metakaolin is clearly evident. Notably, the specimen S1P3K exhibited the highest modulus of elasticity, irrespective of the sand grain size. This is because tiny particles can grow the stiffness of the material by filling holes and reducing defects [51–53]. Besides, three factors can be used to characterize metakaolin's beneficial impacts on foam concrete: the filling effect, the chemical reaction, and the aggregate reinforcement. The filling effect of metakaolin effectively compensates for internal imperfections within the matrix, while its high specific surface area facilitates the formation of strong compounds through chemical reactions. These mechanisms collectively enhance the stiffness and stability of the foamed concrete structure [54,55]. Therefore, metakaolin contributes to increased connectivity and compactness within the composite material, thereby improving the internal microstructure and enhancing the modulus of elasticity. Compared to variations in sand particle size, the incorporation of metakaolin proves to be more effective in augmenting both the elastic modulus and compressive strength [56].

The elastic modulus of foamed concrete is highly dependent on pore size (see Figs. 14 and 16). A material with smaller micropores has a higher elastic modulus. Smaller pores result in a more compact and stiffer structure. When stress is applied, the material with smaller pores exhibits a higher resistance to elastic deformation. For example, in samples where metakaolin is added, the formation of additional hydration products fills the micropores, reducing their size. This leads to an increase in the elastic modulus. As seen in the experimental results, the elastic modulus of S1P3K series samples, which have smaller pores due to metakaolin addition, is higher compared to samples without metakaolin at the same dry density. This is consistent with the general principle that a more refined microstructure with smaller pores leads to a higher elastic modulus. Therefore, a uniform pore distribution results in a more consistent stress response throughout the structure, meaning the material behaves more uniformly under loading. Conversely, non-uniform pore distribution causes variations in material stiffness and leads to heterogeneous stress-strain behavior. Another reason for the high modulus of elasticity for foamed concrete samples containing metakaolin is because its hydration and filling effects reduce pore connectivity, providing a more stable and rigid structure that can better resist deformation.

Furthermore, with respect to the effect of different mix design approaches, no significant changes in elastic modulus were observed across the investigated densities. Therefore, results in terms of elastic modulus are consistent with the outcomes for compressive strength in Section 3.3. Additionally, the linear relationship observed between compressive strength and modulus of elasticity across the series of foamed concrete specimens with varying densities indicates a consistent mechanical response of the material, as plotted in Fig. 15(b). The graph also illustrates that higher elastic modulus values can be achieved for the same compressive strength, suggesting

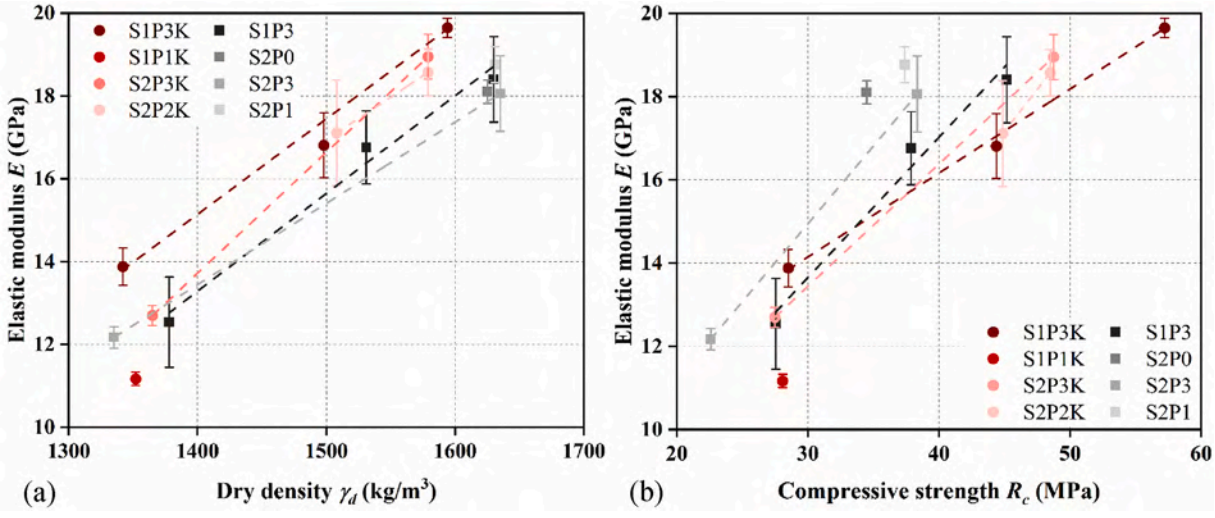

Fig. 15. Effect of dry density on modulus of elasticity for the different foamed concrete investigated (a); compressive strength versus elastic modulus (b).

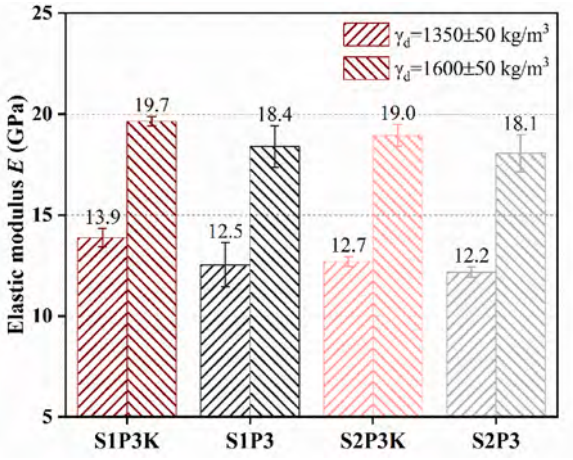

Fig. 16. Effect of the maximum fine sand particle size and of the presence of metakaolin on the elastic modulus of foamed concrete at a target density of 1350 ± 50 kg/m^3 and 1600 ± 50 kg/m^3.

that certain mix designs may effectively enhance elastic modulus. However, it is important to note that these higher elastic moduli were obtained at increased densities, which diminishes a key advantage of using this material: its lightweight nature. Consequently, while the elastic modulus versus compressive strength graph is valuable for understanding the relationship between these two material properties, it is essential to also consider density in the design process, as it plays a critical role in material performance. Lastly, it is important to emphasize the experimental finding that the presence of metakaolin does not result in a reduction of the elastic modulus. This outcome contrasts with the findings in Ref. [46], where the addition of mineral components, specifically fly ash, led to a decrease in the elastic modulus of foamed concrete. This finding in Ref. [46] contrasted with the improvement in compressive strength, resulting in a foamed concrete that, while demonstrating enhanced compressive strength, also exhibited a reduction in elastic modulus, which, at a density of approximately 1600 kg/m^3, was around 10 MPa. Consequently, this led to increased deformability of the structural elements made from that material. In the present study, the inclusion of metakaolin consistently enhances the mechanical properties of the material, ensuring not only improved mechanical performance in terms of compressive and flexural strength but also reduced deformability. Additionally, the foamed concrete presented in this work exhibits superior compressive strength and comparable elastic modulus at the same density, i.e. about 20 GPa at 1600 kg/m^3, when compared to lightweight aggregate concrete, such as the ones with expanded clay. The latter is a material commonly used in practice for the construction of lighter structural elements. Therefore, the material described in this study possesses all the necessary mechanical properties to be effectively utilized in the production of structural components. Ongoing experiments are assessing the material's properties at various densities, focusing on durability and interaction with reinforcement bars. These findings, which will be published in a forthcoming study, will further validate the material's suitability for structural applications.

4. Analytical regression curves

The regression curves are developed for forecasting purposes by analyzing the experimental data presented in the previous sections. It is important to keep in mind that the prediction curves are limited to the range of dry densities examined in this experimental investigation and are only applicable to foamed concrete samples with features comparable to those shown here. From individual measurements, a linear regression curve can roughly describe the observed trend in the dry density of the specimens. As a result, a very classical linear regression equation $y = \alpha + \beta x$ was used for all samples.

The coefficient factors of α and β for the variation of flexural strength R_f, compressive strength R_c, and elastic modulus E with density are given in Table 5, Tables 6, and Table 8, accompanying by the coefficient of determination (CoD) R^2. Tables 7 and 9 represent the flexural-compressive relationship and the compressive-modulus of elasticity relationships. The value of R^2 ranges from 0 to 1. The closer its value is to 1 the better the linear regression matches the observations and vice versa. In the context of this

Table 5
Evaluation of coefficients of the regression curves for flexural strength.

Code ID	Grain size/mm	Metakaolin	SPs dose/%	α coefficient	β coefficient	R^2 value
S1P3K	0.25	1	3.5	−1.223	0.006	0.92
S1P1K	0.25	1	1.5	–	–	–
S1P3	0.25	0	3.5	−9.035	0.010	0.99
S2P3K	0.5	1	3.5	−4.677	0.007	1.00
S2P2K	0.5	1	2	−2.968	0.006	1.00
S2P3	0.5	0	3.5	−5.146	0.008	1.00

Table 6
Evaluation of coefficients of the regression curves for compressive strength.

Code ID	Grain size/mm	Metakaolin	SPs dose/%	α coefficient	β coefficient	R^2 value
S1P3K	0.25	1	3.5	−124.283	0.113	0.98
S1P1K	0.25	1	1.5	–	–	–
S1P3	0.25	0	3.5	−67.864	0.069	0.99
S2P3K	0.5	1	3.5	−88.418	0.086	1.00
S2P2K	0.5	1	2	−32.239	0.051	1.00
S2P3	0.5	0	3.5	−58.848	0.063	1.00

Table 7
Evaluation of coefficients of the regression curves for flexural-compressive strength.

Code ID	Grain size/mm	Metakaolin	SPs dose/%	α coefficient	β coefficient	R^2 value
S1P3K	0.25	1	3.5	−90.640	18.163	0.97
S1P1K	0.25	1	1.5	–	–	–
S1P3	0.25	0	3.5	−7.065	6.736	0.99
S2P3K	0.5	1	3.5	−44.015	13.723	1.00
S2P2K	0.5	1	2	5.960	8.854	1.00
S2P3	0.5	0	3.5	−11.949	6.908	1.00

Table 8
Evaluation of coefficients of the regression curves for elastic modulus.

Code ID	Grain size/mm	Metakaolin	SPs dose/%	α coefficient	β coefficient	R^2 value
S1P3K	0.25	1	3.5	−17.154	0.023	0.99
S1P1K	0.25	1	1.5	–	–	–
S1P3	0.25	0	3.5	−19.751	0.024	0.96
S2P3K	0.5	1	3.5	−27.166	0.029	1.00
S2P2K	0.5	1	2	−13.900	0.021	1.00
S2P3	0.5	0	3.5	−14.041	0.020	1.00

Table 9
Evaluation of coefficients of the regression curves for compressive strength-elastic modulus.

Code ID	Grain size/mm	Metakaolin	SPs dose/%	α coefficient	β coefficient	R^2 value
S1P3K	0.25	1	3.5	8.089	0.202	0.99
S1P1K	0.25	1	1.5	–	–	–
S1P3	0.25	0	3.5	3.539	0.337	0.94
S2P3K	0.5	1	3.5	4.625	0.294	1.00
S2P2K	0.5	1	2	−0.933	0.402	1.00
S2P3	0.5	0	3.5	3.722	0.374	1.00

investigation, linear interpolation is a fair hypothesis to reflect the fluctuation of values including R_f, R_c, and E with density because all samples have extremely strong fitting capacity, and more precisely, because their R^2 values are above 0.95, except for the dry density and flexural strength fitting results for S1P3K (i.e., 0.92). Thanks to the negative value of the coefficient of α, it is evident that the limiting anticipated strength at zero density is negative; nonetheless, this is merely a modeling result with little physical importance [15]. It is emphasized that the suggested linear regression equation can only be used if they cover the range of densities that have been examined in this work. The cases of S2P3K, S2P2K and S2P3 are represented by only two values of densities, therefore a linear curve results in a coefficient of determination R^2 equal to 1. Moreover, for the series S1P1K only one density has been investigated, therefore no regression curve is suggested.

5. Concluding remarks

This study presented an experimental campaign that includes eight series of three different target densities, resulting in a total of 90 foamed concrete samples. The investigation focuses on how metakaolin addition, superplasticizer content, fine aggregate particle size, and dry density influence the flowability of fresh pastes, as well as the development of flexural and compressive strengths and the modulus of elasticity at 28 days. Specifically, the study considered three dry densities (1350, 1500, and 1600 kg/m^3), four superplasticizer dosages (0.75 %, 1.5 %, 2 %, and 3.5 % of cement weight), two different maximum particle size of fine sand (0.25 mm and 0.5 mm), and the incorporation of metakaolin as a partial replacement of sand. The study showed that the slump values of the different series of foamed concrete decrease as the target density of the samples increases. Moreover, for a given density, increasing the fine

aggregate particle size to 0.5 mm can significantly enhance the slump of the foamed concrete. Notably, the study highlights that employing a high superplasticizer dosage (3.5 % of cement weight), combined with a partial replacement of fine sand with metakaolin and a reduced maximum sand particle size (0.25 mm), not only results in self-compacting foamed concrete, but also improves the mechanical performance for all analyzed densities. These strategies enhance the microstructure of the material by reducing pore size. In fact, increasing the superplasticizer-to-cement ratio while reducing the water + foam-to-cement ratio results in an average increase of over 18 % in flexural strength, while reducing the maximum aggregate diameter from 0.5 mm to 0.25 mm results in an average increase in compressive strength of approximately 18 % across all evaluations. However, the primary effect is attributed to the presence of metakaolin, resulting in a contextual average increase of 15 %, 16 %, and 6 % for flexural strength, compressive strength, and elastic modulus, respectively. This is a crucial result because it highlights how contextual improvement of the different quantities investigated can be achieved, enabling the production of foamed concrete with not only improved mechanical properties but also reduced deformability. Achieving flexural strength above 8 MPa, compressive strength exceeding 57 MPa, and an elastic modulus nearing 20 GPa at a density of approximately 1600 kg/m^3 suggests that, with the strategies outlined in this study, this material holds strong potential for structural applications. In conclusion, to fully consider this material suitable for producing structural elements on par with lightweight aggregate concretes, further evaluations are required beyond the scope of this study. In particular, additional research is underway on the durability properties of this material and its interaction with reinforcing bars, which will be published in a forthcoming study.

CRediT authorship contribution statement

Peng Shi: Writing – review & editing, Writing – original draft, Methodology, Investigation, Formal analysis, Data curation. **Devid Falliano:** Writing – review & editing, Writing – original draft, Methodology, Formal analysis, Data curation, Conceptualization. **Qiyun Zhang:** Writing – review & editing, Writing – original draft, Investigation. **Giuseppe Carlo Marano:** Writing – review & editing, Validation, Supervision. **Giuseppe Andrea Ferro:** Writing – review & editing, Validation, Supervision. **Luciana Restuccia:** Writing – review & editing, Validation, Supervision.

Funding sources

Peng Shi gratefully acknowledges the support from the China Scholarship Council (No. 202106650016). The work of Devid Falliano was carried out within the Ministerial Decree no. 1062/2021 and received funding from the FSE REACT-EU – PON Ricerca e Innovazione 2014–2020.

Declaration of competing interest

The authors declare that they have no known competing financial interests or personal relationships that could have appeared to influence the work reported in this paper.

Acknowledgements

The authors would like to express their gratitude to Isoltech Srl for supplying the foaming agent and the metakaolin, with special thanks to Dr. Andrea Bellotti, the company's president, for his valuable recommendations. The authors would like to extend their gratitude to Master Builders Solutions for supplying the superplasticizer, especially to Dr. Sandro Moro for his invaluable advice. Additionally, the authors wish to thank Mr. Ernesto Gugliandolo for his support and valuable suggestions during the research activities and Mrs. Adriana Carolina Bravo Celi for her assistance during the initial experimental investigations.

Data availability

Data will be made available on request.

References

[1] C. Shi, A.F. Jiménez, A. Palomo, New cements for the 21st century: the pursuit of an alternative to Portland cement, Cement Concr. Res. 41 (7) (2011) 750–763.
[2] P.R. Kumar, Low carbonizing cement and concrete industry: a state-of-art review on quaternary blended sustainable self-compacting concrete, Innovative Infrastructure Solutions 10 (2) (2025) 1–13, https://doi.org/10.1007/s41062-025-01865-7.
[3] Z. Yang, P. Shi, Y. Zhang, Z. Li, Effect of superabsorbent polymer introduction on properties of alkali-activated slag mortar, Constr. Build. Mater. 340 (2022) 127541, https://doi.org/10.1016/j.conbuildmat.2022.127541.
[4] Z. Yang, P. Shi, Y. Zhang, Z. Li, Influence of liquid-binder ratio on the performance of alkali-activated slag mortar with superabsorbent polymer, J. Build. Eng. 48 (2022) 103934, https://doi.org/10.1016/j.jobe.2021.103934.
[5] B. Yuan, J. Liang, X. Huang, Q. Huang, B. Zhang, G. Yang, P. Yuan, Eco-efficient recycling of engineering muck for manufacturing low-carbon geopolymers assessed through LCA: exploring the impact of synthesis conditions on performance, Acta Geotechnica (2024) 1–21, https://doi.org/10.1007/s11440-024-02395-9.
[6] V. Pitre, H. La, J.A. Bergerson, Impacts of alternative fuel combustion in cement manufacturing: life cycle greenhouse gas, biogenic carbon, and criteria air contaminant emissions, J. Clean. Prod. 475 (2024) 143717, https://doi.org/10.1016/j.jclepro.2024.143717.
[7] B. Yuan, W. Chen, Z. Li, J. Zhao, Q. Luo, W. Chen, T. Chen, Sustainability of the polymer SH reinforced recycled granite residual soil: properties, physicochemical mechanism, and applications, J. Soils Sediments 23 (1) (2023) 246–262, https://doi.org/10.1007/s11368-022-03294-w.

[8] A.M. Mohamed, B.A. Tayeh, S.S. Majeed, Y.I.A. Aisheh, M.N.A. Salih, Ultra-light foamed concrete mechanical properties and thermal insulation perspective: a comprehensive review, J. CO2 Util. 83 (2024) 102827, https://doi.org/10.1016/j.jcou.2024.102827.

[9] B.P.R.V.S. Priyatham, M.T.S. Lakshmayya, D.V.S.R.K. Chaitanya, Review on performance and sustainability of foam concrete, Mater. Today Proc. (2023), https://doi.org/10.1016/j.matpr.2023.04.080.

[10] W. Huang, X. Chen, L. Feng, T. Ji, Y. Ning, J. Wang, Experimental investigation of mechanical behavior and microstructural properties in roadbed foam concrete at different densities and correlation analysis, Case Stud. Constr. Mater. 19 (2023) e02565, https://doi.org/10.1016/j.cscm.2023.e02565.

[11] D. Falliano, S. Parmigiani, D. Suarez-Riera, G.A. Ferro, L. Restuccia, Stability, flexural behavior and compressive strength of ultra-lightweight fiber-reinforced foamed concrete with dry density lower than 100 kg/m^3, J. Build. Eng. 51 (2022) 104329, https://doi.org/10.1016/j.jobe.2022.104329.

[12] Y. Peng, X. Yuan, L. Jiang, J. Yang, Z. Liu, Y. Zhao, H. Chen, The fabricating methods, properties and engineering applications of foamed concrete with polyurethane: a review, Int. J. Environ. Sci. Technol. 20 (2) (2023) 2293–2312, https://doi.org/10.1007/s13762-022-04115-w.

[13] Y. Liu, Z. Zhao, M.N. Amin, B. Ahmed, K. Khan, S.U. Arifeen, F. Althoey, Foam concrete for lightweight construction applications: a comprehensive review of the research development and material characteristics, Rev. Adv. Mater. Sci. 63 (1) (2024) 20240022, https://doi.org/10.1515/rams-2024-0022.

[14] D. Falliano, L. Restuccia, A. Vinci, G.A. Ferro, Structural foamed concrete: preliminary studies for applications in seismic areas, Procedia Struct. Integr. 44 (2023) 2350–2355, https://doi.org/10.1016/j.prostr.2023.01.300.

[15] D. Falliano, D. De Domenico, G. Ricciardi, E. Gugliandolo, Experimental investigation on the compressive strength of foamed concrete: effect of curing conditions, cement type, foaming agent and dry density, Constr. Build. Mater. 165 (2018) 735–749, https://doi.org/10.1016/j.conbuildmat.2017.12.241.

[16] UNI EN 196-1, Methods of Testing Cement - Part 1, Determination of strength, 2016.

[17] G. Ghahremani, A. Bagheri, H. Zanganeh, The effect of size and shape of pores on the prediction model of compressive strength of foamed concrete, Constr. Build. Mater. 371 (2023) 130720, https://doi.org/10.1016/j.conbuildmat.2023.130720.

[18] British Standard, BS-EN197-1:2011 (2011) Cement-Part 1: Composition, Specifications and Conformity Criteria for Common Cements, BSI.

[19] EN 480-1 (2015) Admixtures for Concrete, Mortar and grout-test methods-part 1: Reference Concrete and Reference Mortar for Testing. Spanish Association for Standardisation and Certification (AENOR), Spain.

[20] UNI EN 934-2, Admixtures for Concrete, Mortar and grout-part 2: Concrete admixtures-definitions, Requirements, Conformity, Marking and Labelling, Publisher: Italian National Unification Agency, 2012.

[21] D. Falliano, E. Gugliandolo, D. De Domenico, G. Ricciardi, Experimental investigation on the mechanical strength and thermal conductivity of extrudable foamed concrete and preliminary views on its potential application in 3D printed multilayer insulating panels, in: T. Wangler, R. Flatt (Eds.), First RILEM International Conference on Concrete and Digital Fabrication - Digital Concrete 2018. DC 2018, vol. 19, RILEM Bookseries, 2019, pp. 277–286, https://doi.org/10.1007/978-3-319-99519-9_26. Springer, Cham.

[22] L.G. Li, B.F. Xiao, J. Yu, Fresh behaviours of glass fibre reinforced mortar: experimental study and modeling based on average water film thickness and fibre/cement ratio, Adv. Cement Res. (2024) 1–32, https://doi.org/10.1680/jadcr.24.00026.

[23] J. Mao, Q. Wang, L. Qu, H. Zhang, Z. Shi, S. Xu, X. Li, Study of mortar layer property of superhydrophobic metakaolin based cement mortar, J. Build. Eng. 45 (2022) 103578, https://doi.org/10.1016/j.jobe.2021.103578.

[24] Q. Li, Y. Fan, Rheological evaluation of nano-metakaolin cement pastes based on the water film thickness, Constr. Build. Mater. 324 (2022) 126517, https://doi.org/10.1016/j.conbuildmat.2022.126517.

[25] L. Lei, T. Hirata, J. Plank, 40 years of PCE superplasticizers-History, current state-of-the-art and an outlook, Cement Concr. Res. 157 (2022) 106826, https://doi.org/10.1016/j.cemconres.2022.106826.

[26] B. Arulmoly, C. Konthesingha, Pertinence of alternative fine aggregates for concrete and mortar: a brief review on river sand substitutions, Aust. J. Civ. Eng. 20 (2) (2022) 272–307, https://doi.org/10.1080/14488353.2021.1971596.

[27] A. Al-Shwaiter, H. Awang, M.A. Khalaf, The influence of superplasticiser on mechanical, transport and microstructure properties of foam concrete, J. King Saud Univ. Eng. Sci. 35 (2) (2023) 101–109, https://doi.org/10.1016/j.jksues.2021.02.010.

[28] Z. Xie, S. Zuo, L. Chen, F. Zhong, Y. Tian, Q. Yuan, Improving the air bubble stability of air-entrained mortar in low air pressure environments via adopted rheology and surface tension methods, Cement Concr. Compos. 150 (2024) 105579, https://doi.org/10.1016/j.cemconcomp.2024.105579.

[29] O. Gencel, T. Bilir, Z. Bademler, T. Ozbakkaloglu, A detailed review on foam concrete composites: ingredients, properties, and microstructure, Appl. Sci. 12 (11) (2022) 5752, https://doi.org/10.3390/app12115752.

[30] D. Falliano, S. Quattrocchi, D. De Domenico, G. Ricciardi, E. Gugliandolo, Critical assessment of CO_2 emission of different concretes: foamed, lightweight aggregate, recycled and ordinary concrete, Acta Polytechnica CTU Proceedings 33 (2022) 153–159, https://doi.org/10.14311/APP.2022.33.0153.

[31] T. Tasiopoulou, D. Katsourinis, D. Giannopoulos, M. Founti, Production-process simulation and life-cycle assessment of metakaolin as supplementary cementitious material, Eng 4 (1) (2023) 761–779, https://doi.org/10.3390/eng4010046.

[32] C. Schiefer, J. Plank, On the CO_2 footprint of polycarboxylate superplasticizers (PCEs) and its impact on the eco balance of concrete, Constr. Build. Mater. 409 (2023) 133944, https://doi.org/10.1016/j.conbuildmat.2023.133944.

[33] S. Prakasan, S. Palaniappan, R. Gettu, Study of energy use and CO_2 Emissions in the manufacturing of clinker and cement, J. Inst. Eng.: Series A 101 (2020) 221–232, https://doi.org/10.1016/j.cemconres.2003.12.020.

[34] A.S. Krishna, R. Siempu, G.S. Kumar, Study on the fresh and hardened properties of foam concrete incorporating fly ash, Mater. Today Proc. 46 (2021) 8639–8644.

[35] UNI EN 13412:2007, Products and Systems for the Protection and Repair of Concrete structures-Test methods-Determination of Modulus of Elasticity in Compression.

[36] R. Rosidawani, H. Hanafiah, Y. Idris, R. Adhitama, M. Hidayat, Strength performance of lightweight aerated concrete on different types of sand and curing method, AIP Conf. Proc. 2689 (1) (2023, July), https://doi.org/10.1063/5.0116549. AIP Publishing.

[37] Y. Qian, K. Lesage, K. El Cheikh, G. De Schutter, Effect of polycarboxylate ether superplasticizer (PCE) on dynamic yield stress, thixotropy and flocculation state of fresh cement pastes in consideration of the critical Micelle Concentration (CMC), Cement Concr. Res. 107 (2018) 75–84, https://doi.org/10.1016/j.cemconres.2018.02.019.

[38] Y. Aygörmez, An experimental study on silica fume and metakaolin doped portland cement-based mortars using silica aerogel and air-entraining admixture, Innovative Infrastructure Solutions 7 (3) (2022) 223, https://doi.org/10.1007/s41062-022-00825-9.

[39] D.L. Pillay, O.B. Olalusi, M.W. Kiliswa, P.O. Awoyera, J.T. Kolawole, A.J. Babafemi, Engineering performance of metakaolin based concrete, Cleaner Engineering and Technology 6 (2022) 100383, https://doi.org/10.1016/j.clet.2021.100383.

[40] P. Dinakar, S.N. Manu, Concrete mix design for high strength self-compacting concrete using metakaolin, Mater. Des. 60 (2014) 661–668, https://doi.org/10.1016/j.matdes.2014.03.053.

[41] A. Al-Shwaiter, H. Awang, M.A. Khalaf, The influence of superplasticiser on mechanical, transport and microstructure properties of foam concrete, J. King Saud Univ. Eng. Sci. (2021), https://doi.org/10.1016/j.jksues.2021.02.010.

[42] I. Abdullaev, U. Abdullaev, The influence of superplasticizers on the porous structure and thermal conductivity of lime foam concrete waste, E3S Web of Conferences 452 (2023) 06013, https://doi.org/10.1051/e3sconf/202345206013. EDP Sciences.

[43] A.N. Shankar, S. Chopade, R. Srinivas, N.K. Mishra, H.K. Eftikhaar, G. Sethi, B. Singh, Physical and mechanical properties of foamed concrete, a literature review, Mater. Today Proc. (2023), https://doi.org/10.1016/j.matpr.2023.10.105.

[44] E.K. Nambiar, K. Ramamurthy, Air-void characterisation of foam concrete, Cement Concr. Res. 37 (2) (2007) 221–230, https://doi.org/10.1016/j.cemconres.2006.10.009.

[45] P. Shi, D. Falliano, A.B. Celi, Z. Yang, G.C. Marano, B. Briseghella, Workability and mechanical properties of structural foamed concretes with different dry densities, and fine sand grain sizes: preliminary Study, in: 2024 IEEE International Workshop on Metrology for Living Environment (MetroLivEnv), 2024, June, pp. 379–383, https://doi.org/10.1109/MetroLivEnv60384.2024.10615453. IEEE.

[46] K. Khan, M.A.M. Johari, M.N. Amin, M. Nasir, Development and evaluation of basaltic volcanic ash based high performance concrete incorporating metakaolin, micro and nano-silica, Developments in the Built Environment 17 (2024) 100330, https://doi.org/10.1016/j.dibe.2024.100330.
[47] H. Jia, J. Zeng, Q. Zou, L. Zheng, R. Pan, Fluorine-free foaming extinguishing agent: design route, fire extinguishing performance, foam stability mechanism, Arab. J. Chem. 17 (4) (2024) 105712, https://doi.org/10.1016/j.arabjc.2024.105712.
[48] N. Narayanan, K. Ramamurthy, Structure and properties of aerated concrete: a review, Cement Concr. Compos. 22 (5) (2000) 321–329, https://doi.org/10.1016/S0958-9465(00)00016-0.
[49] E.P. Kearsley, P.J. Wainwright, The effect of porosity on the strength of foamed concrete, Cement Concr. Res. 32 (2) (2002) 233–239, https://doi.org/10.1016/S0008-8846(01)00665-2.
[50] E.T. Dawood, A.J. Hamad, Toughness behaviour of high-performance lightweight foamed concrete reinforced with hybrid fibres, Struct. Concr. 16 (4) (2015) 496–507, https://doi.org/10.1002/suco.201400087.
[51] Y. Song, D. Lange, Influence of fine inclusions on the morphology and mechanical performance of lightweight foam concrete, Cement Concr. Compos. 124 (2021) 104264, https://doi.org/10.1016/j.cemconcomp.2021.104264.
[52] K. Dhasindrakrishna, K. Pasupathy, S. Ramakrishnan, J. Sanjayan, Progress, current thinking and challenges in geopolymer foam concrete technology, Cement Concr. Compos. 116 (2021) 103886, https://doi.org/10.1016/j.cemconcomp.2020.103886.
[53] V. Kočí, R. Černý, Directly foamed geopolymers: a review of recent studies, Cement Concr. Compos. 130 (2022) 104530, https://doi.org/10.1016/j.cemconcomp.2022.104530.
[54] M. Amran, S.S. Huang, S. Debbarma, R.S. Rashid, Fire resistance of geopolymer concrete: a critical review, Constr. Build. Mater. 324 (2022) 126722, https://doi.org/10.1016/j.conbuildmat.2022.126722.
[55] D. Chen, Y. Zhang, W. Wang, Y. Shi, J. Mao, Y. Liu, S. Chen, Influence of direct foaming methods on the early performance and microstructure of metakaolin-based foam geopolymers, Int. J. Appl. Ceram. Technol. 22 (1) (2025) e14848, https://doi.org/10.1111/ijac.14848.
[56] B. Sankar, P. Ramadoss, Assessment of mechanical and durability performance of silica fume and metakaolin as cementitious materials in high-performance concrete, International Review of Applied Sciences and Engineering 15 (1) (2024) 44–54, https://doi.org/10.1556/1848.2023.00638.